Vol. 52: 193–211, 2012
doi: 10.3354/cr01044

CLIMATE RESEARCH
Clim Res

Published March 22

Contribution to CR Special 29 'The regional climate model RegCM4'

Large-scale origins of rainfall and temperature bias in high-resolution simulations over southern Africa

M. B. Sylla[1,*], F. Giorgi[1], F. Stordal[2]

[1]Earth System Physics (ESP) Section, International Centre for Theoretical Physics (ICTP), PO Box 586, 34151 Trieste, Italy
[2]Department of Geosciences, University of Oslo, Box 1047 Blindern, 0316 Oslo, Norway

ABSTRACT: We use the Abdus Salam International Centre for Theoretical Physics (ICTP) regional climate model, RegCM3, nested in NCEP and ERA-Interim reanalyses (NC-RegCM and ERA-RegCM, respectively) to explore the effect of large-scale forcings on the model biases over a southern Africa domain at 25 km grid spacing. RegCM3 shows a generally good performance in simulating the location of the main rainfall features, temperature and synoptic scale circulation patterns, along with cloud cover and surface radiation fluxes. However, it shows a wet bias which varies substantially when fields from the 2 reanalysis products are used to drive the model, being greater in NC-RegCM than in ERA-RegCM. The wetter bias in NC-RegCM originates from larger moisture inflow, amplified cloud cover and upward motion caused by stronger low-level convergence. Similarly, negative temperature biases are present over most of the land areas, and the wetter NC-RegCM exhibits larger magnitudes of temperature bias. Surface flux analysis reveals that these lower temperature values in the NCEP-driven experiment are due primarily to the surface latent heat flux rather than cloud radiative forcing. As a result, the hydrologic cycle is more intense in the NC-RegCM than in the ERA-RegCM. Our results are relevant for a better understanding of the propagation of errors from the large-scale forcings to the regional model over the region of interest.

KEY WORDS: Rainfall bias · Large-scale conditions · Surface radiation budget · Surface climate

1. INTRODUCTION

Due to the predominance of rain-fed agriculture in southern Africa, our ability to provide rainfall information is important for the economies and societies of the region (Mason & Jury 1997, McGregor 1997, Jury 2002, Reason & Jagadheesha 2005). Impact studies aimed at estimating the consequences of climate change on water resources and agriculture over the region require information at regional to local scales and, hence, an understanding of the main processes regulating climate variability under both present-day and future forcings.

Regional Climate Models (RCMs) (Giorgi & Mearns 1999) are now extensively used to downscale large-scale climate information to regional scales in order to account for fine-scale processes that regulate the spatial structure of climate variables. This is particularly the case for precipitation, which shows complex spatial patterns in regions of steep topography gradients such as southern Africa. Another expectation from RCMs is that the physical and dynamical processes controlling rainfall may be improved at high resolution (Giorgi et al. 1998, Duffy et al. 2006). RCMs have also been used to carry out a wide range of process studies over different southern African domains, such as the impact of soil moisture initialization (Moufouma-Okia & Rowell 2010), domain size (Landman et al. 2005, Browne & Sylla 2011), convection and other physical parameterizations (Pohl et al. 2011, Sylla et al. 2011) and lateral boundary forcings (Sylla et al. 2009, Cerezo-Mota et al. 2011).

*Email: syllabamba@yahoo.fr

One key problem in the simulation of rainfall over the southern African region is the existence of significant biases in RCMs (Engelbrecht et al. 2002, Giorgi 2005, Liang et al. 2008). In particular, a number of previous studies have shown substantial overestimates of precipitation over the near-equatorial convergence zone for both the winter and summer seasons (Joubert et al. 1999, Tadross et al. 2006, Engelbrecht et al. 2009, MacKellar et al. 2009, Tummon et al. 2010). Such deficiency may be derived from the inability of the models to correctly simulate realistic large-scale conditions or to properly respond to such conditions via their convective parameterization (Crétat et al. 2012). Therefore, a contribution to the biases may be derived from lateral boundary forcing (Staniforth 1997, Noguer et al. 1998). As a matter of fact, Sylla et al. (2010a) argued that the specification of lateral boundary conditions of sufficient quality can improve RCM simulations of convection over Africa.

Systematic errors in precipitation and cloud cover will then affect, and feedback with, the surface energy and water budgets. Cloud cover and surface properties influence the net short-wave and long-wave fluxes at the surface, while precipitation provides an essential source for the soil water reservoir (Pal et al. 2000, Tadross et al. 2006). As a result, precipitation and clouds are critical in determining the partitioning of incoming solar radiation into surface sensible and latent heat fluxes (Stephens 2005, Wild et al. 2008). The existence of rainfall biases thus translates into an inaccurate simulation of the surface radiation and water budgets that may be transferred to the hydrology and crop models used for impact studies (Iizumi et al. 2010). An understanding of the nature of such biases can thus help us to improve climate model simulations and avoid the propagation of errors to application models.

In the current paper, we present an analysis of a high-resolution (25 km) version of the International Centre for Theoretical Physics (ICTP) Regional Climate Model 3 (RegCM3) (Pal et al. 2007) nested in the National Center for Environmental Predictions (NCEP; Kalnay et al. 1996) and the European Center for Medium Range Weather Forecast (ECMWF) ERA-Interim (Uppala et al. 2008) reanalyses. In this regard, we stress that the reanalysis from 1979 onwards also incorporates satellite data which have substantially improved the products for the southern hemisphere and in particular southern Africa (Tennant 2004). Differences between these 2 reanalysis products provide a good opportunity to explore how the large-scale environment described by forcing lateral meteorological fields impacts the RCM rainfall and temperature biases, and to investigate their relationship with the surface radiation budget and near-surface climates. In addition, we use the same model configuration presented previously by Sylla et al. (2010a), who used an all-African domain at a 50 km grid interval and lateral driving data from the same ERA-Interim reanalysis used here; this allows us to compare our results with those from this previous work.

The simulations were completed as part of Phase I of the SOCOCA project (Socioeconomic Consequences of Climate Change in sub-equatorial Africa, www.mn.uio.no/geo/english/research/projects/sococa/index.html) in which a series of high-resolution RCM projections are planned in order to assess the effects of climate change on agriculture, air quality and water resources over the region. Therefore, an assessment of the model performance in simulating precipitation and the surface energy budget is important not only for a better interpretation of the projections, but also to establish whether and how the model output needs to be processed to correct relevant biases before use in relevant impact models (e.g. Piani et al. 2010).

In Section 2, we first describe our model, experimental design and analysis strategy. In Section 3, the model results are discussed, and the main conclusions are presented in Section 4.

2. MODEL DESCRIPTION AND SIMULATION DESIGN

The ICTP, RegCM3 (Giorgi et al. 1993a,b, Pal et al. 2007) is a primitive equation, sigma vertical coordinate model based on the hydrostatic dynamical core of the National Centre for Atmospheric Research/Pennsylvania State University's mesoscale meteorological model Version 5 (NCAR/PSU's MM5; Grell et al. 1994). Radiation is represented by the CCM3 (Community Climate Model) parameterization by Kiehl et al. (1996), and the planetary boundary layer scheme follows Holtslag et al. (1990). Interactions between the land surface and the atmosphere are described using the Biosphere Atmosphere Transfer Scheme (BATS1E; Dickinson et al. 1993), while the scheme of Zeng et al. (1998) is used to represent fluxes from ocean surfaces. Convective precipitation is calculated with the scheme of Grell et al. (1994) applying the Fritsch & Chappell (1980) closure assumption. Resolvable precipitation processes are treated with the subgrid explicit moisture scheme (SUBEX) of Pal et al. (2000), which is a physically based parameterization including subgrid-scale cloud fraction, cloud water accretion and evaporation of falling rain-

drops. The model has been used for a wide range of applications (Giorgi & Mearns 1999, Giorgi et al. 2006), including simulations over different African domains (e.g. Anyah & Semazzi 2007, Pal et al. 2007, Abiodun et al. 2008, Kgatuke et al. 2008, Sylla et al. 2010b,c, Mariotti et al. 2011), although at coarser resolution than used here. As mentioned, this model configuration is the same as that used by Sylla et al. (2010a), employing 50 km of resolution over a domain encompassing the whole of Africa. The choice of settings in Sylla et al. (2010a) was based on extensive testing and in-depth analysis of the model performance.

Two experiments were conducted and compared. In the first, the model initial and lateral boundary conditions are provided by the 2.5° × 2.5° gridded, 6 h NCEP reanalysis (Kalnay et al. 1996). These data are derived from various observational sources, including a rawinsonde, surface marine and aircraft data, surface land synoptic data, satellite sounder data, special sensing microwave imager and satellite cloud drift winds. Quality control studies were performed on the data, which were assimilated using a numerical prediction model. The second experiment was conducted using initial and lateral boundary conditions from the ERA-Interim 1.5° × 1.5° gridded reanalysis (Uppala et al. 2008), which is the third generation of the ECMWF reanalysis product. The main advances in this reanalysis compared to ERA-40 are: a higher horizontal resolution (0.75° × 0.75° but available also at 1.5° × 1.5° and 2.5° × 2.5°), 4-dimensional variational analysis, a better formulation of background error constraint, a new humidity analysis, improved model physics, a variational bias correction of satellite radiance data and improved fast radiative transfer model (e.g. Uppala et al. 2008). Several problems experienced in the ERA-40 reanalysis were eliminated or substantially improved in the ERA-Interim. In particular, an important improved performance was seen in capturing the humidity and hydrologic cycle over the tropics.

We should emphasize that, since a lack of observational data exists over Africa and the equatorial oceans, the reanalysis products may contain substantial errors that could be transmitted to the regional climate model via the lateral boundaries — especially if they are placed in data-sparse ocean regions. Finally, sea surface temperatures (SSTs) used to force RegCM3 for both experiments were obtained from the National Oceanic and Atmospheric Administration (NOAA) Optimum Interpolation (OI) SST. This OISST analysis is produced monthly on a 1° grid (Reynolds et al. 2002). The boundary conditions and SST are updated 4 times daily in the RegCM3 using the relaxation procedure described by Giorgi et al. (1993b).

Simulated precipitation, temperature and cloud fractional cover from both experiments are compared against observations from the Climatic Research Unit (CRU; Mitchell et al. 2004). The CRU dataset over Africa includes relatively few and only rain-gauge station-based monthly precipitation data for the period 1901–2002 interpolated onto a grid of 0.5° × 0.5°. Although it appears to be coarse and somewhat smoothed, many of the spatial and temporal characteristics of precipitation and temperature variables over southern Africa can, however, be observed in this dataset (Engelbrecht et al. 2002), which is widely used in model performance assessment. The GPCP (Global Precipitation Climatology Project, 2.5° × 2.5° resolution; Adler et al. 2003) product is also used as an additional reference for the baseline validation to account for uncertainties in rainfall observations and to allow extension of the analysis to the surrounding oceans. The atmospheric circulation in the interior domain is compared to the NCEP and the ERA-Interim reanalysis data used to drive the model at the lateral boundaries.

As direct observations of surface radiation fluxes are not available, we use those calculated in the Global Energy and Water Cycle Experiment (GEWEX) Surface Radiation Budget (SRB) program (Darnell et al. 1992, Whitlock et al. 1995, Stackhouse et al. 2004), hereafter referred to as SRB. The SRB (Gupta et al. 2006) provides satellite-based datasets of global short-wave and long-wave radiation components at the earth's surface and at the top of the atmosphere (TOA) on 1° × 1° resolution and monthly scales. These surface radiation fluxes were evaluated in a variety of studies and found to be accurate within an uncertainty range of 5 W m^{-2} and within 5–20 W m^{-2} for, respectively, long-wave and short-wave fluxes (Gupta et al. 1999, Zhang et al. 2006, 2009). From SRB, we also use cloud fraction data (also 1° × 1° resolution and a monthly timescale) which are based on the International Satellite Cloud Climatology Project (ISCCP) (Rossow & Schiffer 1999). We emphasize, however, that the CRU observations and the SRB product are independent datasets and therefore some inconsistency may arise between them.

Both the NC-RegCM and ERA-RegCM experiments are long-term continuous simulations covering the 11 yr period 1990–2000, whereby the first year (1990) is considered spin-up time and is thus not included in the analysis. Although surface outputs are archived every 3 h, minimum and maximum tem-

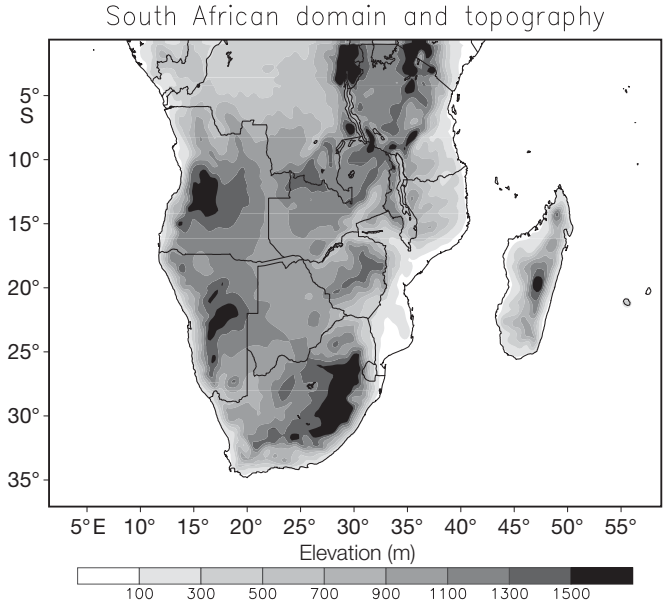

Fig. 1. Southern Africa interior simulation domain and topography

peratures are computed within the code using all time steps. Only the core of the austral summer rainy season, from December through February (DJF), during which the southern African continent region receives >60% of its annual rainfall totals (Engelbrecht et al. 2009), is analyzed. The model domain and topography are shown in Fig. 1. The domain covers the southern African region (south of the equator) and the surrounding ocean areas at a grid spacing of 25 km. Fig. 1 shows that the main features of the southern Africa topography are represented reasonably well. It has been pointed out that it could be ideal for the southern boundary to be located further south to better resolve the waves of the westerly wind regime (Landman et al. 2005), and this will be considered in future experiments. We also note that the domain is extended to the east to account for large-scale features from the Mascarene High across Madagascar towards the southern African continent, which are particularly important for the region's moisture inflow (Landman et al. 2005).

3. RESULTS AND DISCUSSION

3.1. Rainfall and low-level synoptic features

In this section, we first analyze and compare the spatial distribution of mean rainfall and some of the associated synoptic circulation features, such as low-level wind fields, ascent of air and vertically integrated moisture fluxes and convergence. As mentioned, we limit our analysis to the austral summer season (DJF: December–January–February), which is the main rainy season over the southern African continent.

Fig. 2a–d shows mean rainfall from CRU, GPCP and both RegCM3 simulations, respectively. Tables 1–3 report different quantitative performance measures, such as the mean bias (MB), the root mean square difference (RMSD) and the pattern correlation coefficient (PCC) between the simulated and observed variables calculated for the entire land region in the interior domain. For comparison purposes, these quantitative measures are also reported for the 2 reanalysis products and the results of Sylla et al. (2010a), but only for precipitation and temperature. In the observations (CRU and GPCP), rainfall maxima are located within a tilted zonal band encompassing the sub-equatorial southern African region, the Zaire Air Boundary (ZAB) area and the region south of the Congo basin. Although some moderate intensity is found along the Drakensberg mountain range of South Africa, rainfall decreases in the southwestern regions of the domain, where the Kalahari and Namibia deserts experience <1 mm d^{-1} precipitation.

Both the NC-RegCM and ERA-RegCM simulations reproduce the location of the high- and low-intensity rainfall zones with a PCC of about 0.72 and 0.75, respectively. We note that these PCCs are somewhat decreased by the higher spatial detail of the rainfall pattern in the RegCM simulations compared to CRU. In fact, both coarser resolution analyses show greater precipitation PCC, higher than 0.8, while the simulation of Sylla et al. (2010a) had a PCC of 0.75. Finally, the lateral boundary condition forcing does not much affect the simulated spatial precipitation patterns, as a correlation of 0.97 is found between the NCEP-RegCM and ERA-RegCM. This PCC is greater than the PCC between the 2 reanalysis precipitation fields, which, however, remains very high (0.88).

In general, in the RegCM simulations, the peak magnitudes over sub-equatorial Africa, as well as over the southern African subcontinent and the Drakensberg Mountains, are higher than observed. Precipitation differences are highlighted and expressed as percentages in Fig. 3 and as MB and RMSD in Tables 1 & 2, respectively. NC-RegCM overestimates the CRU rainfall by up to 100% (Fig. 3a) over the central regions of southern Africa, while excessive rainfall from ERA-RegCM in the same area does not exceed 50% (Fig. 3b). On the other hand, when averaged over all interior domain land masses, NC-RegCM overestimates precipitation by about 11.6%, while ERA-RegCM underestimates it by about 8%

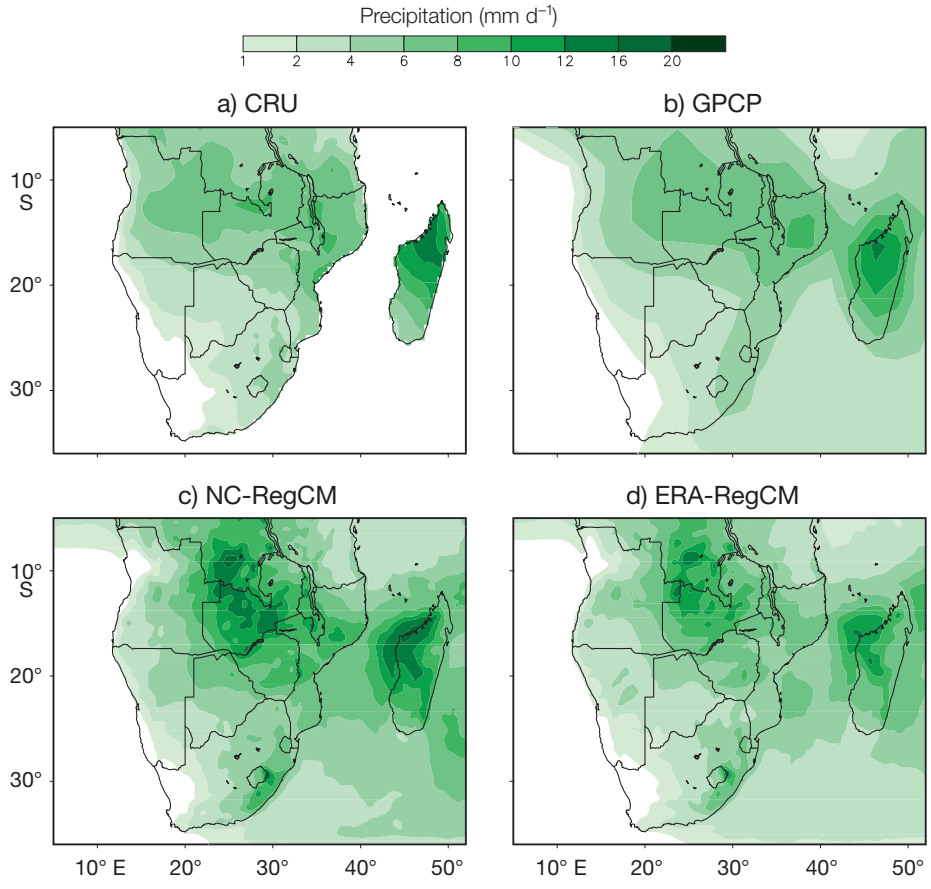

Fig. 2. Mean rainfall climatology (mm d^{-1}) for the period 1991–2000 from (a) CRU, (b) GPCP, (c) NC-RegCM and (d) ERA-RegCM

Table 1. Mean bias between the simulations (NC-RegCM and ERA-RegCM) and the reference CRU observation data (OBS) for precipitation (precip.), mean (T2m), minimum (T2Min) and maximum (T2Max) temperatures, and cloud fractional cover (CF) and GEWEX/SRB data for the downward short-wave (SWD), net short-wave (SWN), downward long-wave (LWD) and net long-wave (LWN) radiation. The values in **bold** for precipitation and temperature are calculated for the corresponding driving field. The values in *italics* are for the ERA-Interim driven experiment of Sylla et al. (2010a)

Variables	Precip. (%)	Temperature (K)			CF (%)	Radiation (W m^{-2})			
		T2m	T2Min	T2Max		SWD	LWD	SWN	LWN
NC-RegCM	11.59	−0.84	−1.37	1.62	−1.25	53.79	−10.38	46.19	8.35
vs. OBS	**7.72**	**−1.78**							
ERA-RegCM	−8.12	−0.67	−1.39	1.89	−5.19	51.63	−13.31	43.94	12.28
vs. OBS	**−16.41**	**−1.13**							
	(*−11.54*)	**(*0.31*)**							
ERA-RegCM	−17.74	0.08	−0.06	0.15	−3.20	−2.21	−2.93	−2.26	3.91
minus NC-RegCM	**−19.79**	**0.53**							

(Table 1). In both cases, the RegCM precipitation is slightly greater than that in the corresponding reanalyses. The better PCCs in the reanalysis fields also contribute to smaller RMSDs than those in the RegCM (Table 2). We also find that, compared to the experiment of Sylla et al. (2010a) (see Table 1), RegCM3 tends to produce more precipitation, which confirms its tendency to yield increased rainfall at higher resolution (e.g. Torma et al. 2011). Tables 1 to 3 thus show that the precipitation fields in the 2 RegCM simulations are generally closer than those in the driving reanalyses. Finally, in both experiments, an underestimation is found in the Atlantic and Indian coastal areas and adjacent interiors between 5° and 20° S.

Table 2. Root mean square difference (RMSD) between the simulations (NC-RegCM and ERA-RegCM) and the reference CRU observation data (OBS) for precipitation (precip.), mean (T2m), minimum (T2Min) and maximum (T2Max) temperatures and cloud fractional cover (CF) and GEWEX/SRB data for the downward short-wave (SWD) net short-wave (SWN), downward long-wave (LWD) and net long-wave (LWN) radiation. The values in **bold** for precipitation and temperature are calculated for the corresponding driving field. The values in *italics* are for the ERA-Interim driven experiment of Sylla et al. (2010a)

Variables	Precip. (mm d^{-1})	Temperature (K)			CF (%)	Radiation (W m^{-2})			
		T2m	T2Min	T2Max		SWD	LWD	SWN	LWN
NC-RegCM	2.01	1.20	1.32	2.01	8.17	26.19	7.04	22.51	8.32
vs. OBS	**1.55**	**1.88**							
ERA-RegCM	1.32	1.11	1.30	2.11	9.81	25.25	7.90	21.42	8.81
vs. OBS	**0.83**	**1.36**							
	(***1.38***)	(***1.24***)							
NC-RegCM	2.69	0.80	0.59	1.02	0.99	14.47	7.61	13.47	10.35
vs. ERA-RegCM	**0.43**	**0.21**							

Table 3. Pattern correlation coefficients (PCC) between the simulations (NC-RegCM and ERA-RegCM) and the reference CRU observation data (OBS) for precipitation (precip.), mean (T2m), minimum (T2Min) and maximum (T2Max) temperatures and cloud fractional cover (CF) and GEWEX/SRB data for the downward short-wave (SWD) net short-wave (SWN), downward long-wave (LWD) and net long-wave (LWN) radiation. The values in **bold** for precipitation and temperature are calculated for the corresponding driving field. The values in *italics* are for the ERA-Interim driven experiment of Sylla et al. (2010a)

Variables	Precip. (mm d^{-1})	Temperature (K)			CF (%)	Radiation (W m^{-2})			
		T2m	T2Min	T2Max		SWD	LWD	SWN	LWN
NC-RegCM	0.72	0.81	0.89	0.65	0.83	0.81	0.86	0.85	0.74
vs. OBS	**0.83**	**0.65**							
ERA-RegCM	0.75	0.83	0.90	0.68	0.85	0.84	0.87	0.87	0.79
vs. OBS	**0.89**	**0.78**							
	(***0.75***)	(***0.81***)							
NC-RegCM	0.97	0.99	0.99	0.99	0.98	0.98	0.99	0.99	0.99
vs. ERA-RegCM	**0.88**	**0.90**							

In summary, it is evident that when driven by the NCEP reanalysis, RegCM3 tends to simulate much higher rainfall totals than when nested within the ERA-Interim reanalysis (Fig. 3c, Table 1), resulting in a larger MB (11.59%) and RMSD (2.01 mm d^{-1}) in NC-RegCM than in ERA-RegCM (–8.32 and 1.32 mm d^{-1}, respectively). This illustrates the strong influence of the lateral meteorological boundary forcing on model behavior (e.g. Giorgi & Mearns 1999).

We thus investigate whether the origin of the precipitation bias and differences across the 2 simulations may be found, at first order, in the synoptic regional circulations derived from the lateral boundary forcings. The 850 hPa wind convergence and superimposed wind vectors are displayed in Fig. 4 for the NCEP and ERA-Interim reanalyses and the 2 RegCM3 simulations, along with their difference. In the reanalyses, strong northeasterly and southeasterly flow from the northern Indian Ocean and Mascarene High converge over central southern Africa, where they also meet the northwesterlies and southerlies from the Atlantic Ocean. This forms a cyclonic pattern around the Angola/Namibia region which has been shown to favor low-level moisture advection (Reason et al. 2006, Vigaud et al. 2009). It is evident that central southern Africa is thus affected by the Inter-Tropical Convergence Zone (ITCZ) in DJF, which explains the maximum rainfall over the region.

Although the wind directions are similar in the NCEP and ERA-Interim reanalyses, the northerlies from the Atlantic and Indian Oceans are stronger in the former, which leads to greater convergence over central southern Africa. The RegCM3 simulations reproduce these low-level circulation features, but the magnitudes and wind convergence are more intense and more sharply defined than in the reanalysis products, which might contribute to explain the greater precipitation in the RegCM3 simulations

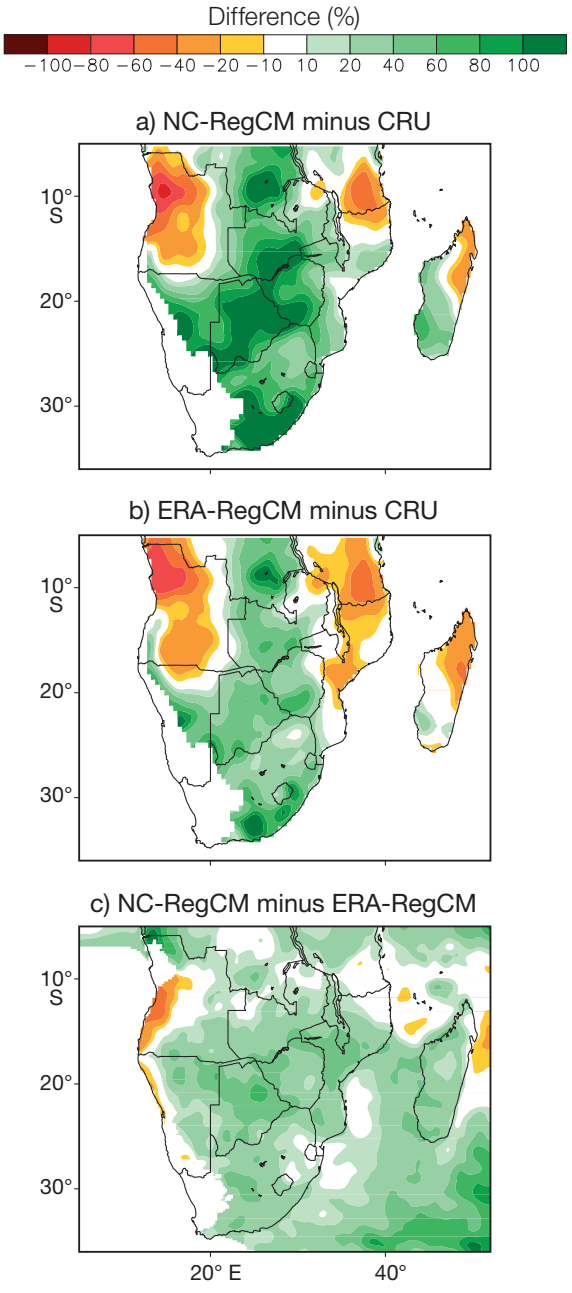

Fig. 3. Differences in mean rainfall climatology compared to CRU for (a) NC-RegCM and (b) ERA-RegCM and (c) the inter-model difference between the 2 simulations. Units for Panels a and b are percentage of observed values and for Panel c percentage of ERA-RegCM values

than in the driving reanalyses (Table 1). This is probably the result of the greater spatial resolution of the regional model. In addition, following reanalysis forcing, the northerly wind cores are once again more intense in NC-RegCM than in ERA-RegCM, indicating enhanced wind convergence in the sub-equatorial southern Africa region as shown in Fig. 4f. Such distribution of the wind convergence strongly impacts the location of ascent of air over the region. In fact, both NCEP and ERA-Interim reanalysis (Fig. 5a,b) show 2 distinct regions of strong upward motion: a lower-level ascent between 35 and 30° S certainly linked to the convection occurring below 900 hPa at the ocean–land interface and along the Drakensberg mountain range; and a deeper core of rising air from the mid- to the upper levels extended along the sub-equatorial southern African regions and related to the occurrence of stronger mass convergence. Both simulations (Fig. 5d,e) capture the location of these 2 cores of upward motion; however, the magnitudes are consistently and substantially greater in NC-RegCM than in ERA-RegCM (Fig. 5f) along all the sub-equatorial southern African regions in response to stronger simulated wind convergence.

The corresponding simulated total moisture transport is illustrated by the vertically integrated zonal and meridional fluxes and moisture convergence. This is shown in Fig. 6 along with their respective differences. Both experiments exhibit similar spatial patterns, with eastward and westward zonal moisture fluxes originating from the tropical Atlantic and the Mascarene High in the Indian Ocean, respectively. The magnitudes, however, are larger in the NC-RegCM simulation. Similarly, the meridional moisture flux component is mostly northerly over land in both runs, but also more intense in NC-RegCM. As a consequence, the magnitude of the total moisture convergence over most of the southern African region is greater in NC-RegCM compared to ERA-RegCM, which is consistent with the stronger lower-level convergence and upward motion.

We thus conclude from our analysis that overall, RegCM3 reproduces the location of the main characteristics of rainfall and circulation features; however, substantial discrepancies exist among the 2 simulations. When the regional model is driven by the ERA-Interim reanalysis it simulates weaker low-level wind convergence, less intense cores of upward motion, lower total moisture fluxes and lower and more realistic rainfall amounts. Therefore, the strength of the low-level mass convergence, which in this model configuration is mostly driven by lateral boundary forcing, is an important factor in determining the location and intensity of precipitation, suggesting the existence of a strong dynamical control mechanism of rainfall in the simulations (see also Tomas & Webster 1997, Biasutti et al. 2006). We also note that the RegCM3 has a tendency to produce more intense precipitation with increased horizontal resolution (e.g. Torma et al. 2011), and this might contribute to the overestimate of precipitation found in these

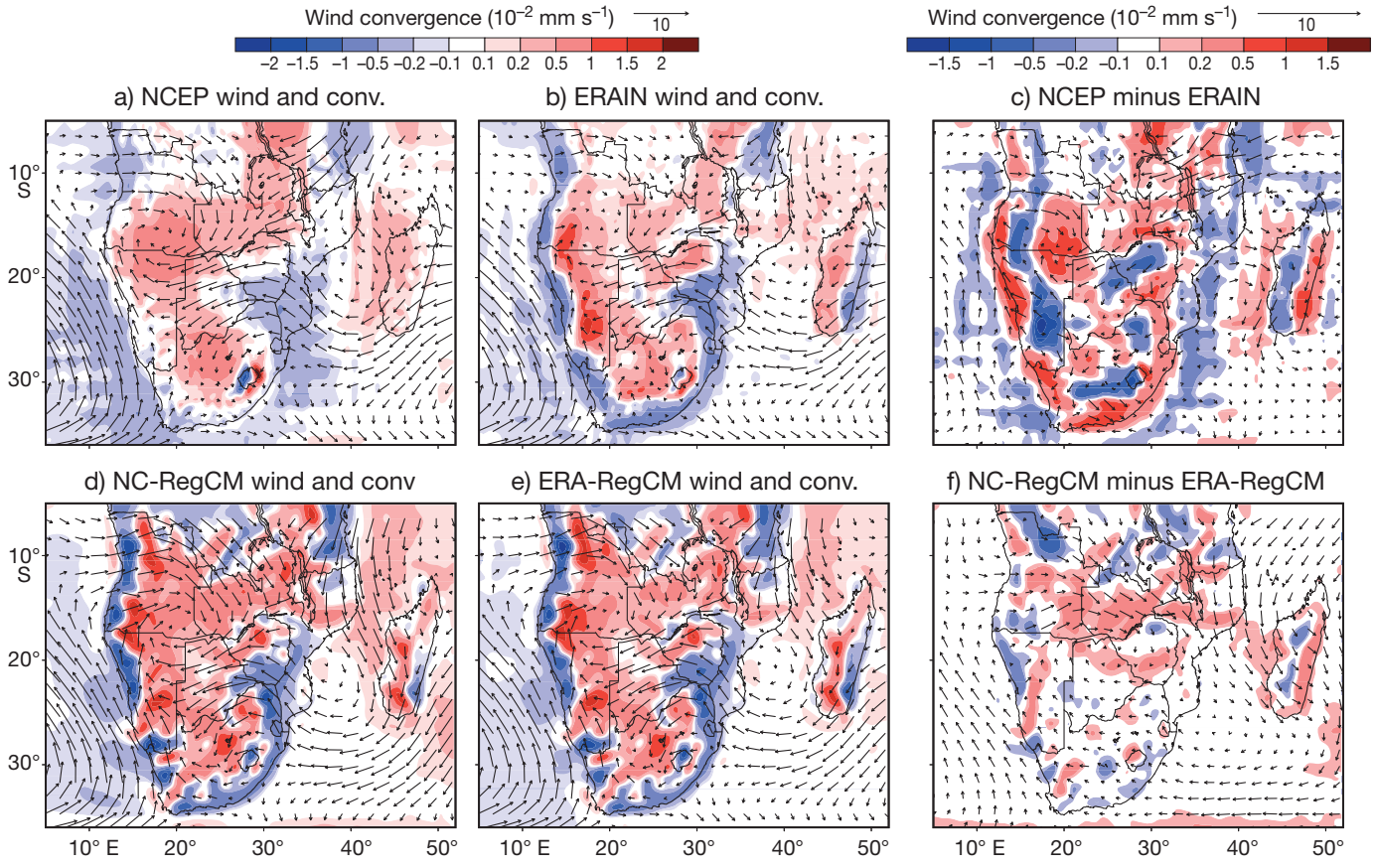

Fig. 4. Mean climatology of low-level (850 hPa) wind convergence (conv.) (10^{-2} mm s^{-1}) and superimposed wind vectors (10 m s^{-1}) for (a) NCEP, (b) ERA-Interim (ERAIN), (c) difference between NCEP and ERA-Interim, (d) NC-RegCM simulation, (e) ERA-RegCM simulation and (f) inter-model difference between NC-RegCM and ERA-RegCM

experiments compared to the previous lower resolution (50 km) simulation of Sylla et al. (2010a). This overestimation can possibly be ameliorated by adjusting different parameters in the RegCM convection and resolved scale precipitation schemes (Giorgi et al. 2012, this special).

3.2. Surface air temperature and cloud cover

Having examined the differences in the simulated circulation features and their impacts on the atmospheric moisture fluxes and rainfall, in this section we investigate how these are related to the simulation of surface temperature and cloud cover.

The spatial distribution of mean DJF surface air temperature from CRU observations, NC-RegCM, ERA-RegCM along with their biases and differences across the 2 simulations (inter-model difference) are displayed in Fig. 7. As for the rainfall, the MB, the RMSD and the PCC between the simulated and the observed temperatures are reported in Tables 1 to 3, respectively. The RegCM simulations capture the temperature maxima over the Kalahari Desert, the Zambezi Valley and along the flatter coastal regions adjacent to the Indian Ocean. Both simulated and observed minima are found over the Drakensberg Mountains. Overall the PCC is >0.8, indicating good agreement between model and observations. Over land areas both simulations exhibit a predominant negative temperature bias, mostly <2°C. The area average of this bias over the entire region, considering only grid points over land, is <1 K (−0.84 and −0.67 K for NC-RegCM and ERA-RegCM, respectively) and it is in fact lower than the corresponding driving fields (−1.78 and −1.13 K for NCEP and ERA-Interim, respectively) and the results by Sylla et al. (2010a). The RegCM3 simulations also exhibit lower RMSD and higher PCC than the corresponding reanalyses (Tables 2 & 3), suggesting a significant added value at higher resolution for this variable. Note that this cold bias in the simulated temperature fields is generally consistent with the corresponding wet rainfall bias. However, although precipitation is certainly an im-

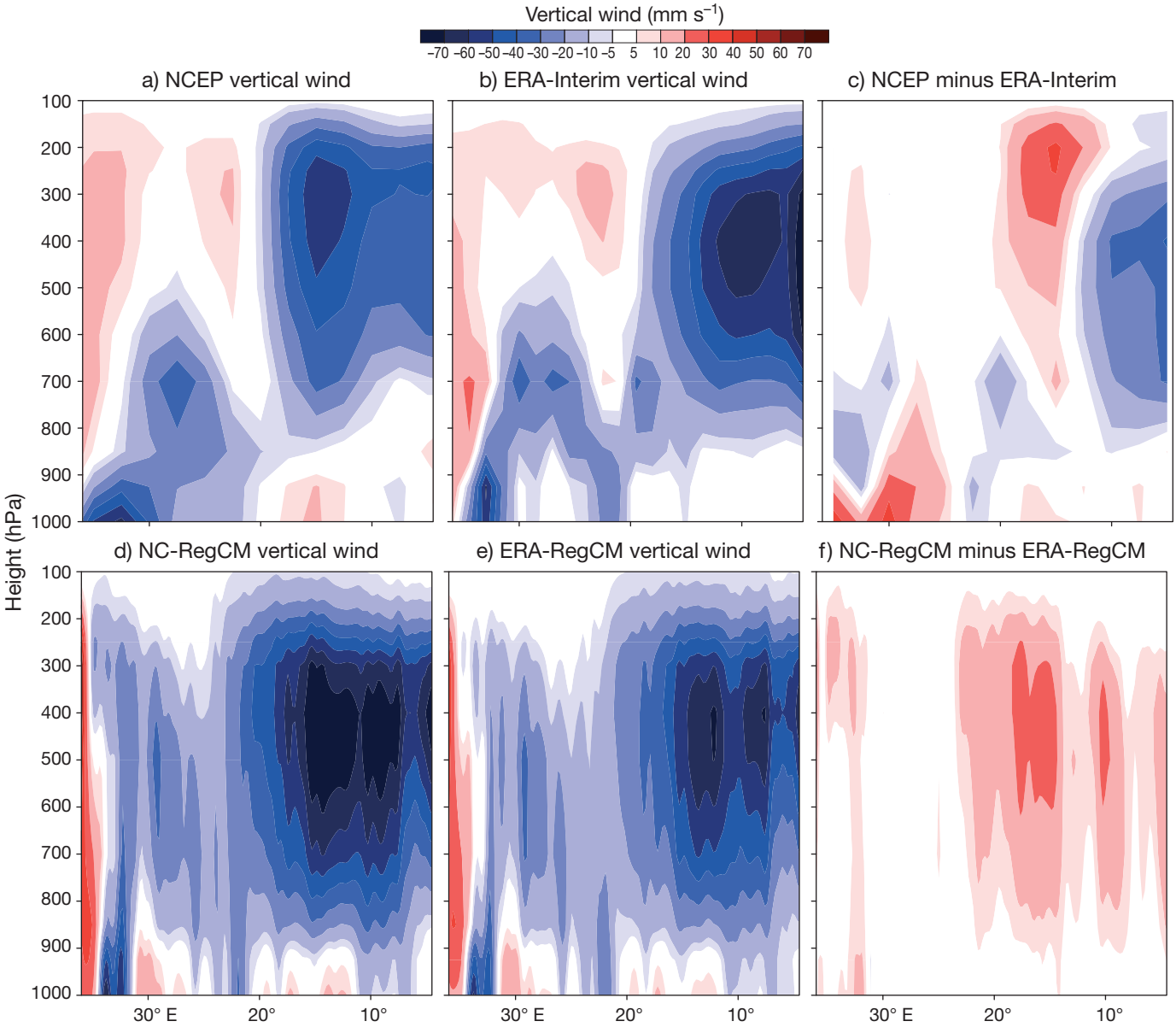

Fig. 5. Latitude–height cross section of the mean climatology of vertical wind (mm s^{-1}) for (a) NCEP, (b) ERA-Interim, (c) difference between NCEP and ERA-Interim, (d) NC-RegCM, (e) ERA-RegCM and (f) inter-model difference between NC-RegCM and ERA-RegCM

portant factor in determining surface temperatures, these cold biases may also result from a combination of different additional elements, including clouds, energy fluxes, surface albedo and temperature advection (Giorgi et al. 1998, Tadross et al. 2006).

Before evaluating these additional factors, it is useful to assess biases in the daily minimum and maximum temperatures. Fig. 8 presents the daily minimum and maximum temperature inter-model difference and their bias (compared to CRU observations), while Tables 1 to 3 summarize, respectively, the MB, the RMSD and the PCC with respect to the CRU observations. We note from Table 1 that, when averaged, minimum temperature shows a negative bias, while maximum temperature shows a positive one. In addition, from Table 3, the PCC indicates better performance for minimum than for maximum temperature. It is also evident from Fig. 8 and Table 1 that the mean temperature cold bias in the interior continental regions (e.g. Fig. 7e,f) is essentially due to a corresponding bias in minimum daily temperature (e.g. Fig. 8b,c). Maximum temperature shows small biases in the continental interior, while the coastal areas and adjacent regions (mainly the western coast of southern Africa) are characterized by warm biases, leading to the overall warm bias and an RMSD of

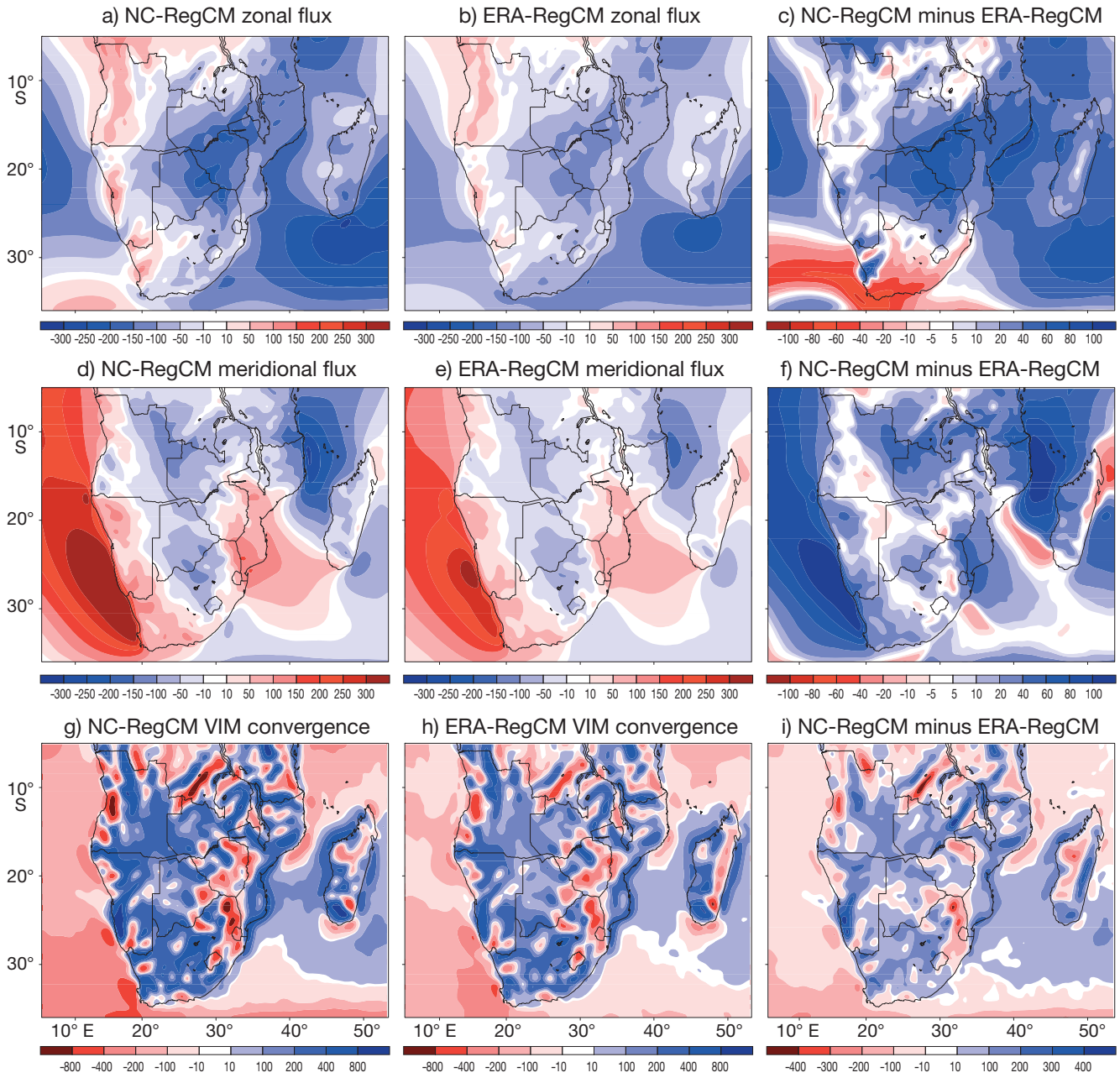

Fig. 6. Mean climatology of vertically integrated zonal moisture flux (upper panels), meridional moisture flux (middle panels) and total moisture convergence (lower panels) for (a,d,g) NC-RegCM, (b,e,h) ERA-RegCM and (c,f,i) inter-model difference in the corresponding absolute values between NC-RegCM and ERA-RegCM. Units for moisture flux (a–f) are kg m^{-1} s^{-1} and for moisture convergence (g–i) are 10^{-3} g m^{-2} s^{-1}

>2 K. In addition, the continental inter-model difference in mean temperature between NC-RegCM and ERA-RegCM is mostly due to a negative inter-model difference in maximum temperature. These results suggest that the minimum temperature cold bias might be related to excessive nighttime infrared loss in both simulations, while the inter-model difference may be more associated with the greater daytime precipitation in the NC-RegCM run (e.g. Fig. A1 in Appendix 1), leading to larger daytime evaporative cooling.

The mean total cloud cover from CRU observations, SRB, NC-RegCM and ERA-RegCM, along with the bias and inter-model difference distributions, are shown in Fig. 9. Good agreement is found between the simulated and observed spatial patterns of cloud cover (PCC of >0.8 for both experiments), with the highest cloud amounts over the sub-equatorial con-

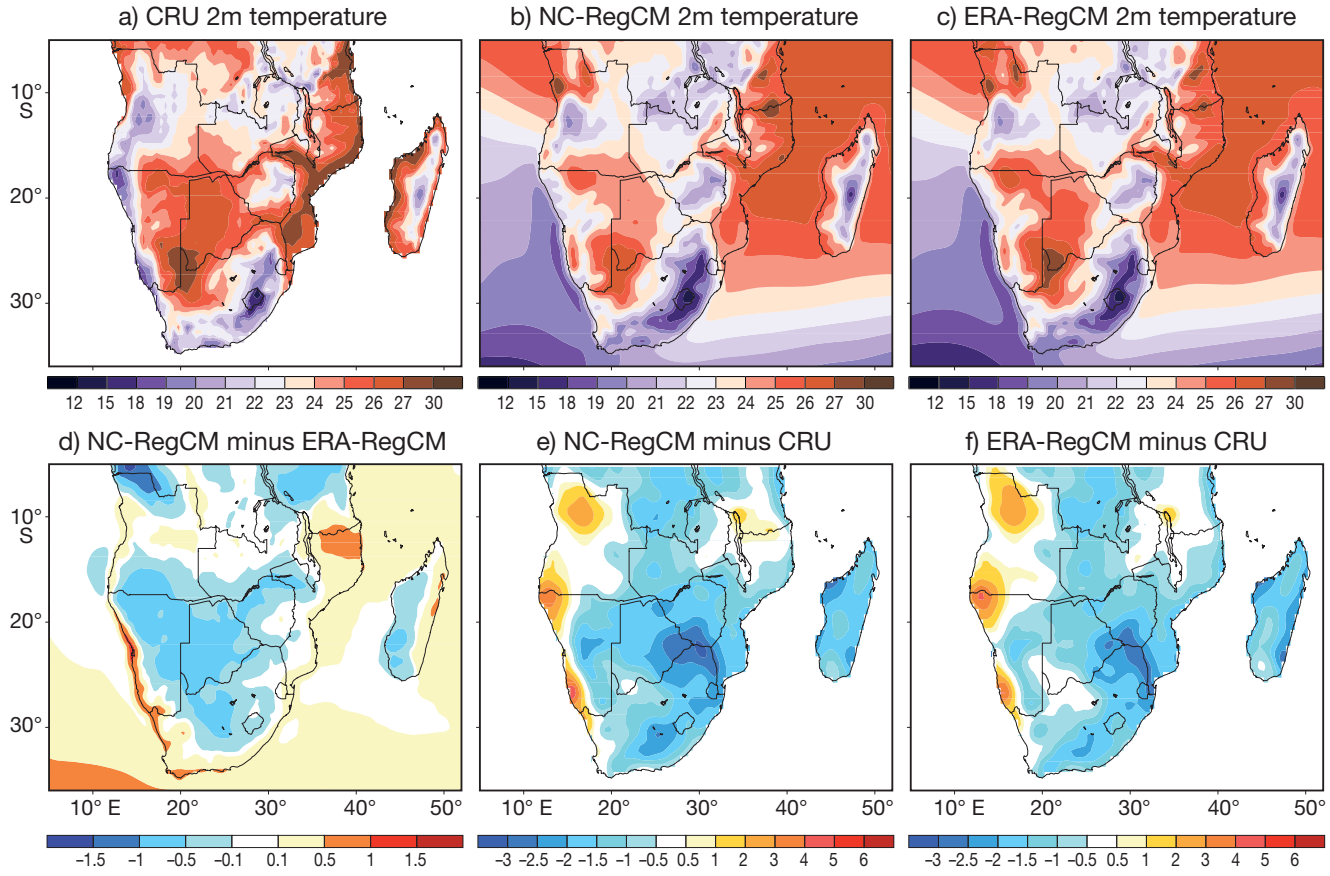

Fig. 7. Mean climatology of 2 m mean temperature (°C) for (a) CRU, (b) NC-RegCM, (c) ERA-RegCM, (d) inter-model difference between NC-RegCM and ERA-RegCM, and bias of (e) NC-RegCM and (f) ERA-RegCM with respect to CRU

vergence zone, the ZAB and south of the Congo basin, and the lowest amounts over the Kalahari Desert. In the subtropics, both runs tend to underestimate fractional cloud cover compared to the SRB product, while they mostly overestimate it compared to CRU observations. This confirms the existence of large uncertainties in the cloud observations and highlights the difficulties in unambiguously assessing the performance of model simulation of cloud cover. For example, the rainfall and temperature distribution would be more consistent with cloud cover from CRU, while the surface radiation budget, with that of the SRB. Therefore, in what follows, we will mostly focus on inter-model differences in order to evaluate the impact of the different simulated cloud amounts on the surface radiation budget and near-surface climates.

When comparing NC-RegCM and ERA-RegCM cloud covers, we find greater values in the former (consistent with the greater total moisture fluxes and precipitation values), and this is also consistent with the lower maximum daily temperatures in the NCEP-driven runs. Therefore, although cloud fractional cover is only one of the factors affecting the surface radiative fluxes, and although significant uncertainties are present in both the simulated and observed estimates of total fractional cloud cover (Rossow & Schiffer 1999), cloudiness appears to be a significant element determining the model surface temperature biases. Given the uncertainties mentioned above, however, the model appears to provide a realistic simulation of cloudiness over the region. The way this affects the surface energy budget is discussed in the next section.

3.3. The surface radiation budget

In an attempt to validate the surface radiation budget and to elucidate the effect of the different components of this budget on the surface climate, we here analyze and compare incident downward and net short-wave and long-wave radiation at the surface. The validation of these radiation variables is performed by comparison with the SRB values. Given the uncertainties in the SRB products, our validation focuses mainly on the comparison between the spa-

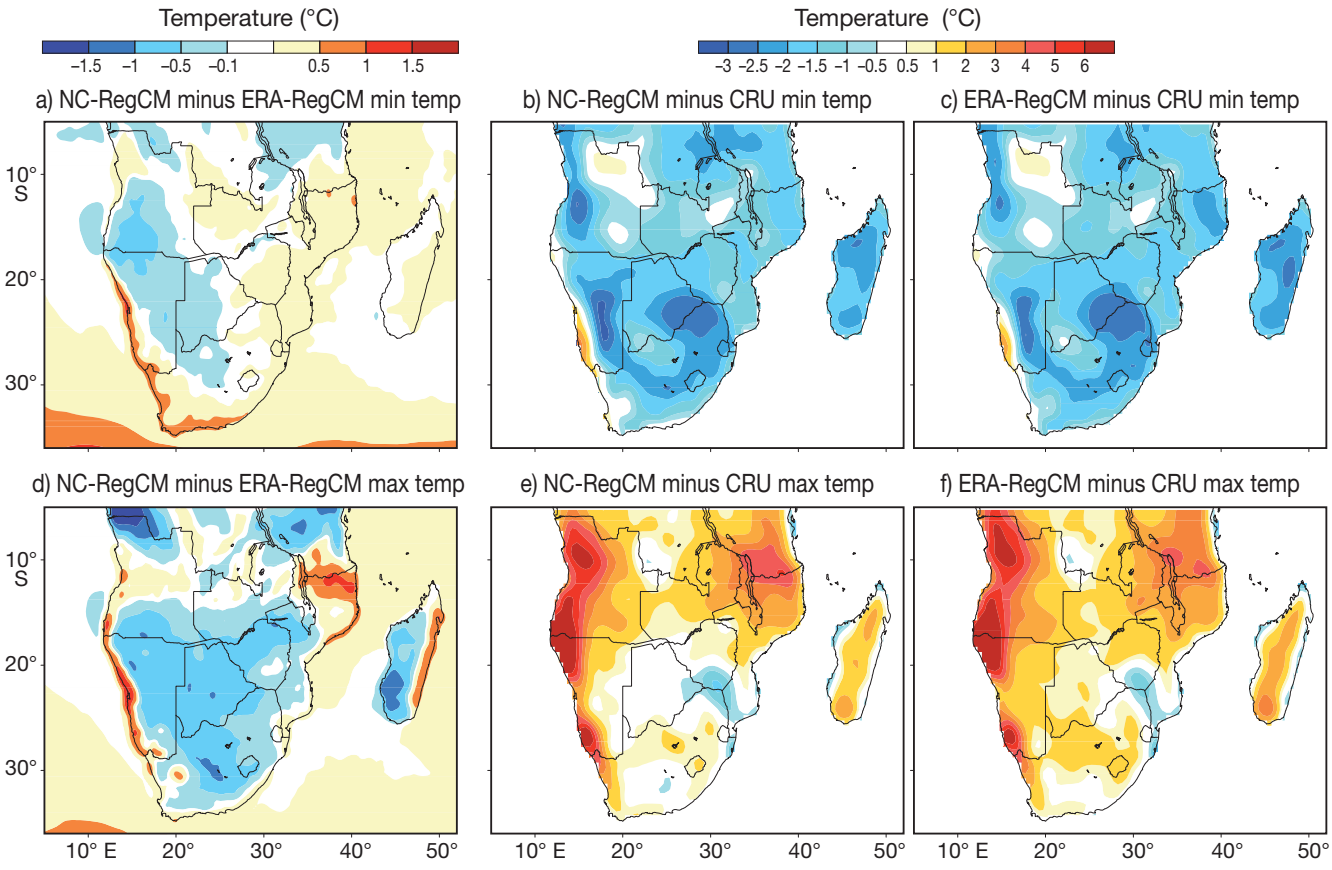

Fig. 8. Minimum daily temperature climatology (upper panels) and maximum daily temperature climatology (lower panels) for (a,d) inter-model difference between NC-RegCM and ERA-RegCM, (b,e) bias of NC-RegCM with respect to CRU and (c,f) bias of ERA-RegCM with respect to CRU

tial patterns of simulated and observed variables, rather than the magnitude of these variables. Their consistency with the cloud fractional cover, temperature and therefore rainfall is assessed by comparing the 2 model simulations.

Fig. 10 shows the surface downward short-wave radiation from the SRB product, NC-RegCM, ERA-RegCM, their biases and inter-model differences. Following the cloud cover distribution inversely, downward short-wave radiation is maximum over the southwestern desert regions and decreases in a northeastward direction to reach a minimum over the Congo basin. Both simulations reproduce the observed spatial patterns, with a PCC >0.8, but systematically overestimate the surface downward solar radiation over land by 10 to 90 W m^{-2} compared to SRB, resulting in a RMSD of >25 W m^{-2}. It should be stressed that our simulations do not incorporate any aerosol forcings, which would result in a greater atmospheric absorption and scattering, thus decreasing the incoming solar radiation flux (Tummon et al. 2010). This could improve the simulation of the short-wave flux and reduce the warm bias found in the maximum daily temperature.

Comparing the 2 simulations, we find that the greater cloud fractional cover in the NC-RegCM run does not lead to a large difference in solar radiation, since most of the difference in cloudiness occurs during the night time (e.g. Fig. A2 in Appendix 1). However, overall, the spatial pattern of the differences in short-wave radiation is consistent with the differences in cloud fractional cover when compared to the SRB data (See Fig. 9e,f). We also note that the spatial distribution of the net absorbed short-wave radiation at the surface from SRB and the simulations (along with their differences) consistently follows the corresponding patterns for incoming solar radiation and therefore is not shown for brevity.

The surface downward and net long-wave radiation patterns are shown in Figs. 11 & 12, respectively. Over most land areas, the bias between the regional model and observed incoming long-wave flux is about 15 W m^{-2}, which is within the estimated uncertainty of the SRB product (Gupta et al. 1999). Largest

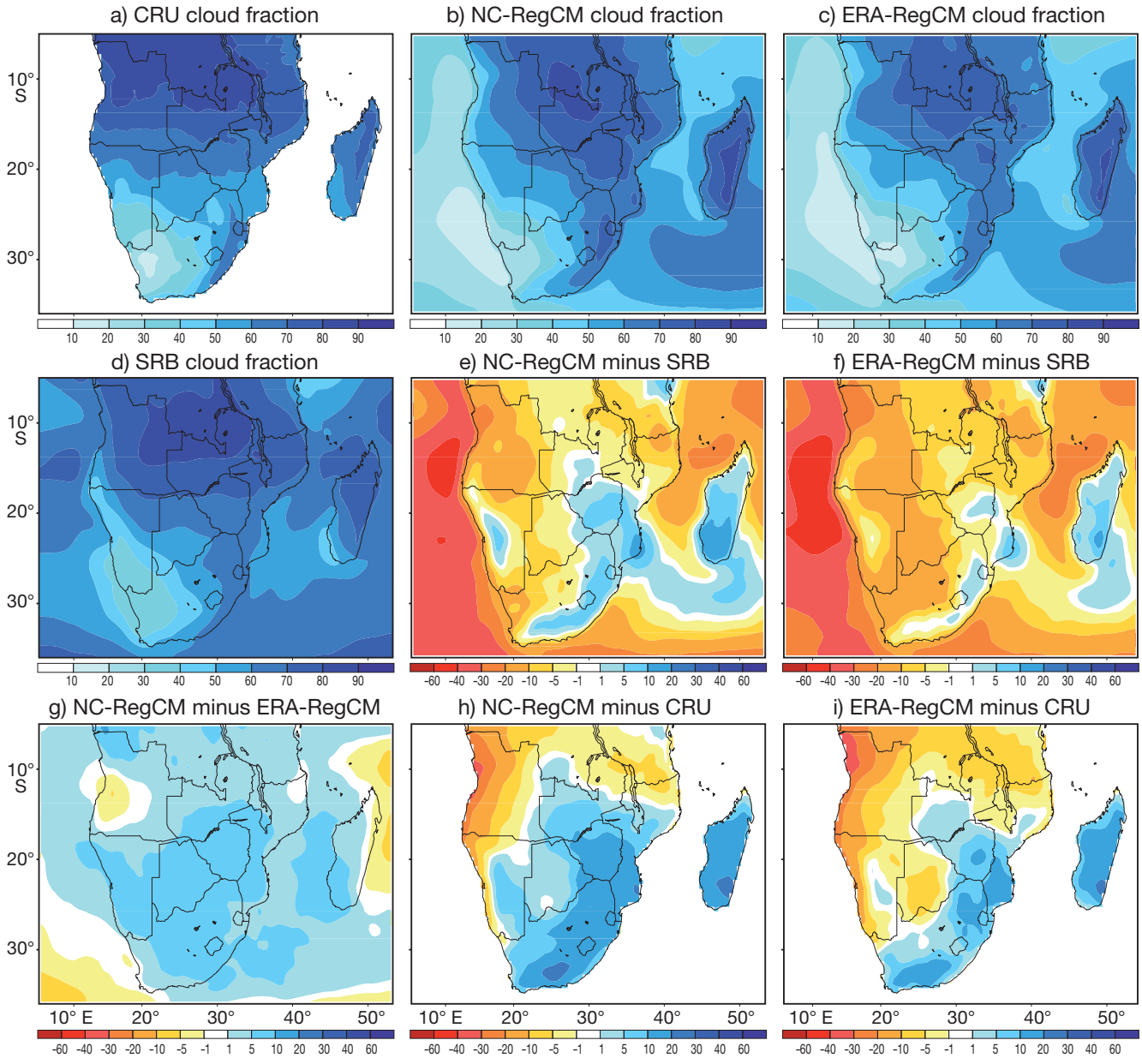

Fig. 9. Mean climatology of cloud fractional cover (in %) for (a) CRU, (b) NC-RegCM, (c) ERA-RegCM, (d) SRB, (e) bias of NC-RegCM with respect to SRB, (f) bias of ERA-RegCM with respect to SRB, (g) inter-model difference between NC-RegCM and ERA-RegCM, (h) bias of NC-RegCM with respect to CRU and (i) bias of ERA-RegCM with respect to CRU

biases are present over the coastal areas and especially the regions adjacent to the Atlantic Ocean. This may be related to the deficiency of the model to produce low level stratus clouds over cold ocean areas (T. A. O'Brien et al. unpubl.). This problem has also been noted in application over the eastern Pacific Ocean off the coasts of California, and a new planetary boundary layer scheme is being implemented in the RegCM system to ameliorate this problem (T. A. O'Brien et al. unpubl.). The inter-model difference is mostly positive, indicating that the simulation with greater cloud amounts (NC-RegCM) yields greater surface long-wave radiation; however, the differences generally appear small.

The corresponding surface net long-wave radiation (Fig. 12), defined as the downward minus upward long-wave radiation at the surface, shows again good spatial agreement between the model and observations, with a PCC of >0.7. The differences between simulated and observed values show a dipolar pattern, with positive values in sub-equatorial regions and negative values in the southern areas of the domain. Systematic lower values along with a lower RMSD are found in NC-RegCM com-

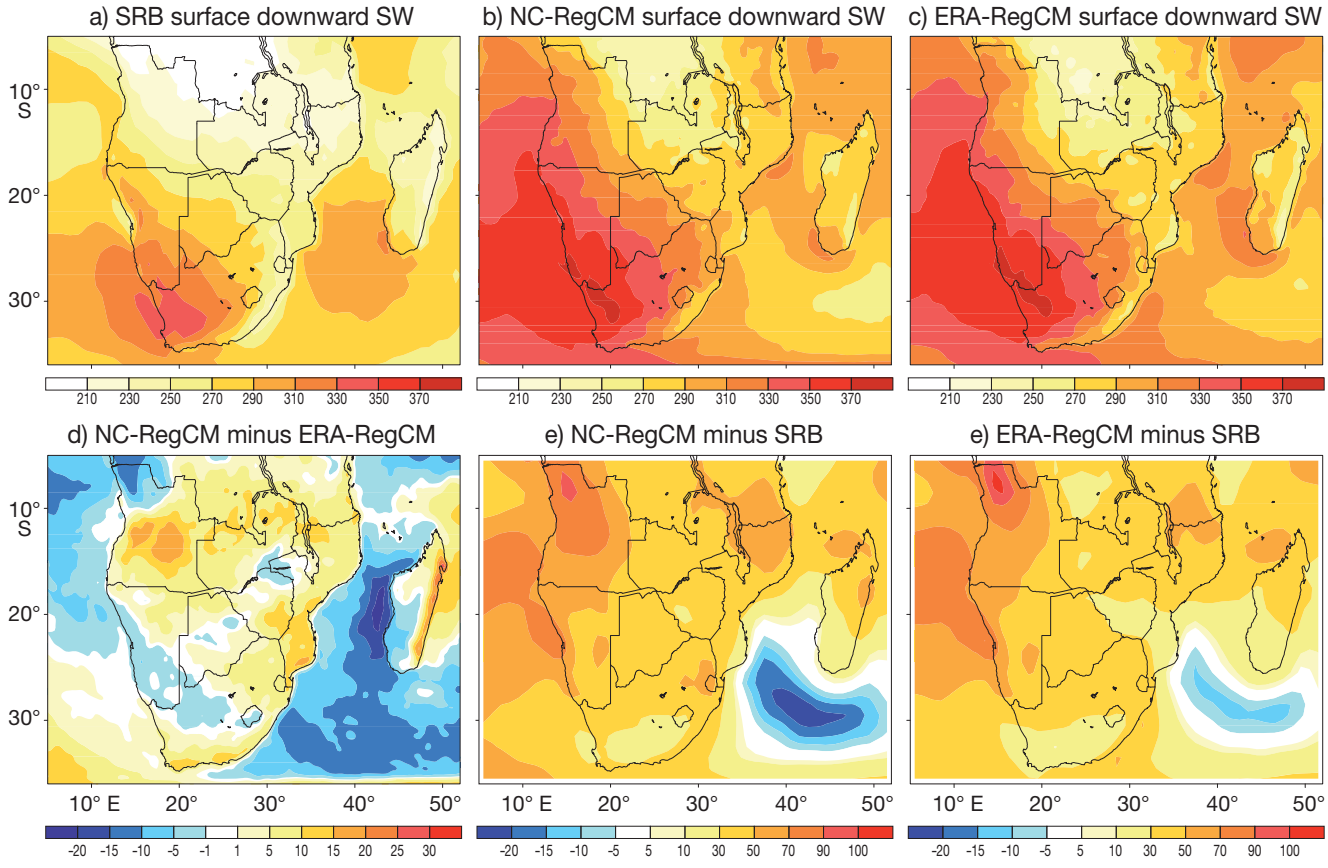

Fig. 10. Mean climatology of surface downward short-wave (SW) radiation flux (W m^{-2}) for (a) SRB, (b) NC-RegCM, (c) ERA-RegCM, (d) inter-model difference between NC-RegCM and ERA-RegCM, (e) bias of NC-RegCM with respect to SRB and (f) bias of ERA-RegCM with respect to SRB

pared to ERA-RegCM, principally because of the lower temperatures (and thus upward long-wave flux) in the former.

The overall comparison of the simulated radiative fluxes with the SRB product shows that RegCM3 captures the spatial patterns of the analyzed surface radiation budget components fairly well with a PCC of 0.7 to 0.8. However, some significant biases appear, such as an overestimation of surface incoming solar, net short-wave and long-wave radiation over most of the land masses and an underestimation of net long-wave radiation over the west coasts and Atlantic Ocean, which is consistent with underestimated cloud amounts compared to the SRB product.

Concerning the radiative flux differences between the 2 model simulations, although for the downward long-wave and short-wave fields these are consistent with the cloudiness field, they are also small (mostly <10 W m^{-2}) and thus do not appear to fully explain the differences in surface air temperature. Other components of the surface energy budget, specifically the surface sensible and latent heat, must thus be important. Fig. 13a,b shows the difference between NC-RegCM and ERA-RegCM sensible and latent heat fluxes, respectively. In the wetter NC-RegCM simulation, the latent heat flux is greater (and the sensible heat flux correspondingly smaller) than in ERA-RegCM by up to 40 W m^{-2} (up to 15 W m^{-2} for sensible heat) because of the higher soil water content (not shown). When comparing these inter-model differences with those of the downward solar and infrared radiation, we thus conclude that the main driver for the different temperature responses in the 2 model runs is latent heat.

4. CONCLUSIONS

In the present paper, we evaluated the performance of a high-resolution version of the ICTP-RegCM3 in reproducing the mean climatology of rainfall, temperature, cloud cover and the surface radiation budget components over southern Africa during the austral summer season. Particularly, we investigated the

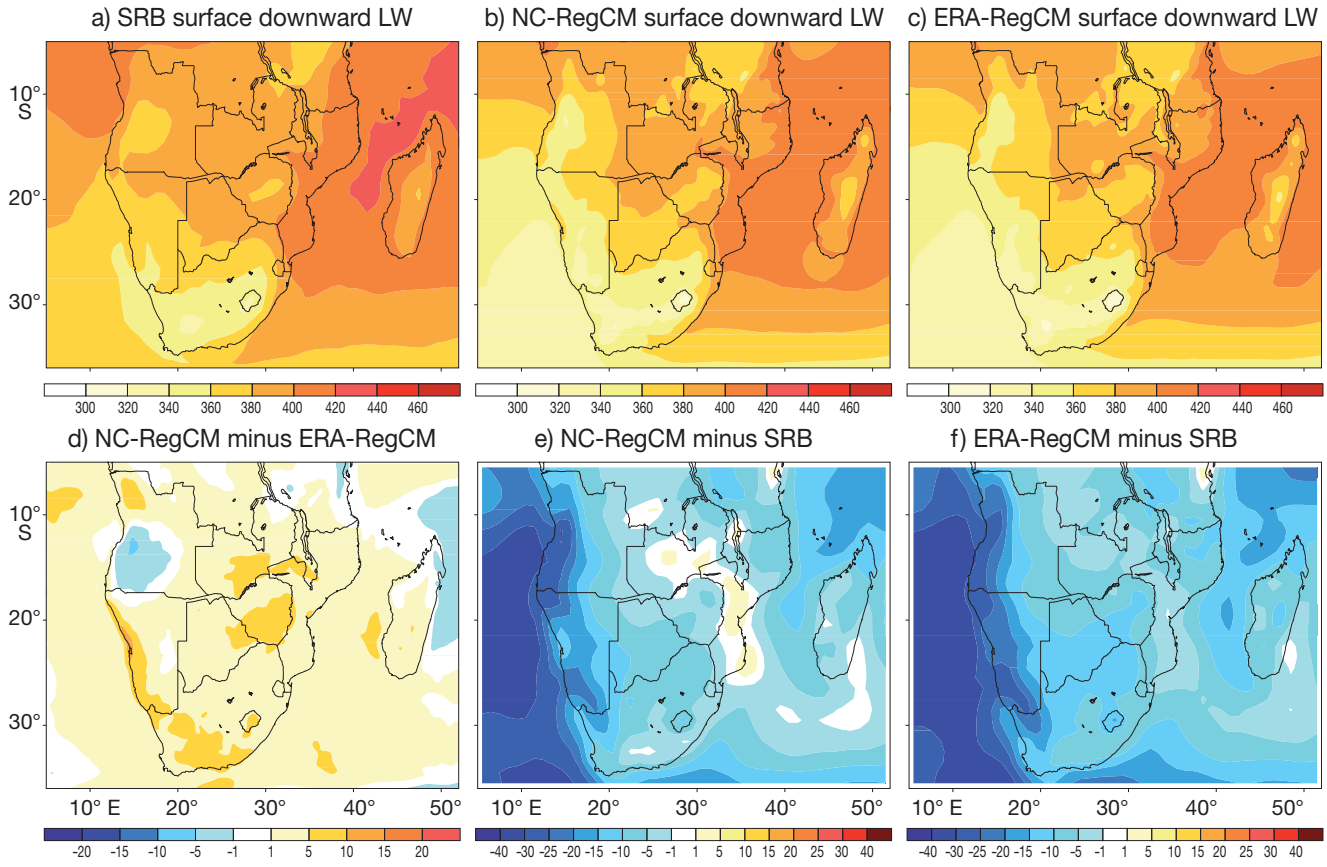

Fig. 11. Mean climatology of surface downward long-wave (LW) radiation flux (W m^{-2}) for (a) SRB, (b) NC-RegCM, (c) ERA-RegCM, (d) inter-model difference between NC-RegCM and ERA-RegCM, (e) bias of NC-RegCM with respect to SRB and (f) bias of ERA-RegCM with respect to SRB

large-scale origins of rainfall and temperature biases and sought to understand their relationship with simulated surface energy budget components. This was achieved through the comparison of 2 simulations, 1 driven by NCEP (NC-RegCM) and 1 driven by ERA-Interim (ERA-RegCM) reanalysis fields.

Our results show that the RegCM3 is able to reproduce the spatial patterns of atmospheric circulation, precipitation, temperature, cloud cover and surface radiative fluxes, with pattern correlation coefficient generally exceeding 0.7. The model, however, exhibits wet biases, which are also tied to the lateral boundary forcing fields. In fact the bias is much larger in the NC-RegCM than the ERA-RegCM, mostly in response to greater zonal and meridional moisture fluxes along with greater low-level wind, upward motion and total moisture convergence over the continental interior in the NCEP reanalysis–driven run. The precipitation overestimate is accompanied by corresponding dominant biases in temperature (cold nighttime minimum temperature conditions and warm maximum temperature bias over coastal areas), cloudiness (underestimate compared to SRB), downward short-wave (overestimate) and downward long-wave (underestimate) radiation. A comparison of the simulated energy budget components, however, indicates that the main driver for the different surface temperature responses in the 2 simulations is latent heat rather than radiative fluxes.

The lack of aerosols likely contributes to some of the overestimate observed in the simulation of short-wave radiative fluxes (Tummon et al. 2010). We also found that for the current model configuration, the ERA-Interim reanalysis provides better quality forcing fields than the NCEP reanalysis. In the present paper, we mostly explored the effect of the forcing lateral boundary fields and did not attempt to specifically tune the model for the present application. The version employed here is the same as used by Sylla et al. (2010a) for an all-Africa domain at coarser horizontal resolution (50 km), which did exhibit a smaller wet bias. This result confirms the tendency of the RegCM3 model to produce greater precipitation amounts at finer horizontal resolutions (Torma et al.

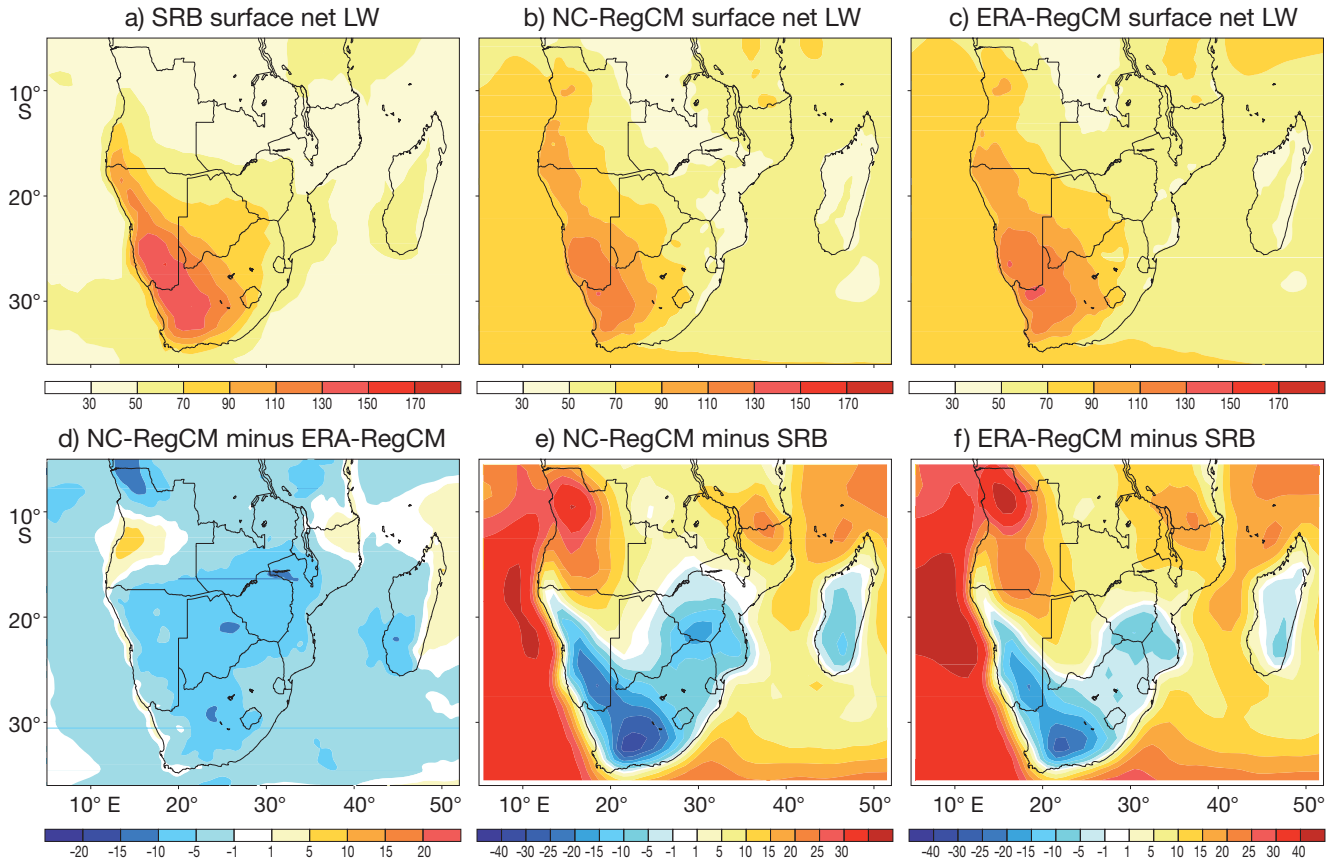

Fig. 12. Mean climatology of surface net long-wave (LW) radiation flux (W m^{-2}) for (a) SRB, (b) NC-RegCM, (c) ERA-RegCM, (d) inter-model difference between NC-RegCM and ERA-RegCM, (e) bias of NC-RegCM with respect to SRB and (f) bias of ERA-RegCM with respect to SRB

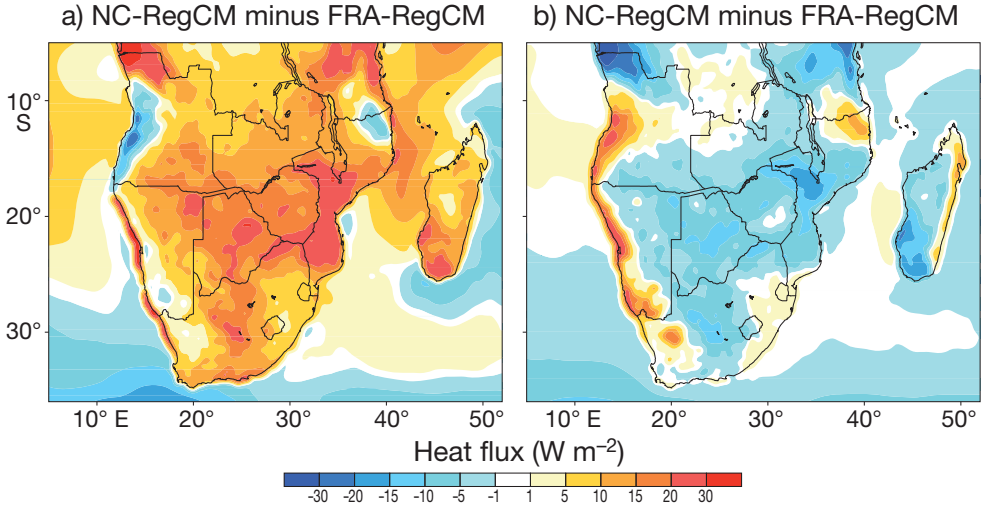

Fig. 13. Mean climatology difference between NC-RegCM and ERA-RegCM for (a) latent and (b) sensible heat flux (W m^{-2})

2011). However, key parameters can be adjusted in both the resolved scale and convective precipitation schemes to optimize model performance (Giorgi et al. 2012). We thus plan to perform such an optimization exercise before applying the latest version of the RegCM model system (RegCM4; Giorgi et al. 2012) to the climate change scenario simulations planned as part of the SOCOCA project.

Acknowledgements. Mouhamadou Bamba Sylla was supported by the Norwegian Research Council FRIMUF program through the SOCOCA project (Socioeconomic Consequences of Climate Change in sub-equatorial Africa).

LITERATURE CITED

Adler RF, Huffmann GJ, Chang A, Ferraro R and others (2003) The version-2 Global Precipitation Climatology Project (GPCP) monthly precipitation analysis (1979–present). J Hydrometeorol 4:1147–1167

Anyah R, Semazzi F (2007) Variability of East African rainfall based on multiyear RegCM3 simulations. Int J Climatol 27:357–371

Biasutti M, Sobel AH, Kushnir Y (2006) AGCM precipitation biases in the tropical Atlantic. J Clim 19:935–958

Browne NAK, Sylla MB (2012) Regional climate model sensitivity to domain size for the simulation of the West African monsoon rainfall. Int J Geophys 2012:625831, doi:10.1155/2012/625831

Cerezo-Mota R, Allen M, Jones R (2011) Mechanisms controlling precipitation in the northern portion of the North American monsoon. J Clim 24:2771–2783

Crétat J, Pohl B, Richard Y, Drobinski P (2012) Uncertainties in simulating regional climate of Southern Africa: sensitivity to physical parameterizations using WRF. Clim Dyn 38:613–634

Darnell WL, Staylor WF, Gupta SK, Ritchey NA, Wilber AC (1992) Seasonal variation of surface radiation budget derived from ISCCP-C1 data. J Geophys Res 97:15741–15760

Dickinson RE, Henderson-Sellers A, Kennedy PJ (1993) Biosphere–Atmosphere Transfer Scheme (BATS) Version 1E as coupled to the NCAR Community Climate Model. Technical Note NCAR/TN–387 + STR, NCAR, Boulder, CO

Duffy PB, Arritt RW, Coquard J, Gutowski W and others (2006) Simulations of present and future climates in the western United States with four nested regional climate models. J Clim 19:873–895

Engelbrecht FA, Rautenbach CJW, McGregor JL, Katzfey JJ (2002) January and July climate simulations over the SADC region using the limited-area model DARLAM. Water SA 28:361–373

Engelbrecht FA, McGregor JL, Engelbrecht CJ (2009) Dynamics of the conformal-cubic atmospheric model projected climate-change signal over southern Africa. Int J Climatol 29:1013–1033

Fritsch JM, Chappell CF (1980) Numerical prediction of convectively driven mesoscale pressure systems. I. Convective parameterization. J Atmos Sci 37:1722–1733

Giorgi F (2005) Climate change prediction. Clim Change 73: 239–265

Giorgi F, Mearns LO (1999) Introduction to special section: regional climate modelling revisited. J Geophys Res 104: 6335–6352

Giorgi F, Marinucci MR, Bates GT (1993a) Development of a second-generation regional climate model (RegCM2). I. Boundary-layer and radiative transfer processes. Mon Weather Rev 121:2794–2813

Giorgi F, Marinucci MR, Bates GT, Canio GD (1993b) Development of a second-generation regional climate model (RegCM2). II. Convective processes and assimilation of lateral boundary conditions. Mon Weather Rev 121: 2814–2832

Giorgi F, Mearns LO, Shields C, McDaniel L (1998) Regional nested model simulations of present day and 2 × CO_2 climate over the Central Plains of the US. Clim Change 40: 457–493

Giorgi F, Coppola E, Solmon F, Mariotti L and others (2012) RegCM4: Model description and preliminary tests over multiple CORDEX domains. Clim Res 52:7–29

Grell GA, Dudhia J, Stauffer DR (1994) Description of the fifth generation Penn State/NCAR Mesoscale Model (MM5). Technical Note NCAR/TN–398 + STR, NCAR, Boulder, CO

Gupta SK, Ritchey NA, Wilber AC, Whitlock CH, Gibson GG, Stackhouse PW Jr (1999) A climatology of surface radiation budget derived from satellite data. J Clim 12: 2691–2710

Gupta SK, Stackhouse PW Jr, Cox SJ, Mikovitz JC, Zhang T (2006) Surface radiation budget project completes 22-year data set. GEWEX WCRP News 16:12–13

Holtslag AAM, De Bruin EIF, Pan HL (1990) A high resolution air mass transformation model for short-range weather forecasting. Mon Weather Rev 118:1561–1575

Iizumi T, Nishimori M, Yokozawa M (2010) Diagnostics of climate model biases in summer temperature and warm-season insolation for the simulation of regional paddy rice yield in Japan. J Clim 49:574–591

Joubert AM, Katzfey JJ, McGregor JL, Nguyen KC (1999) Simulating midsummer climate over southern Africa using a nested regional climate mode. J Geophys Res 104(D16):19015–19025

Jury MR (2002) Economic impacts of climate variability in South Africa and development of resource prediction models. J Appl Meteorol 41:46–55

Kalnay E, Kanamitsu M, Kistler R, Collins W and others (1996) The NCEP/NCAR 40-year reanalysis project. Bull Am Meteorol Soc 77:437–471

Kgatuke MM, Landman WA, Beraki A, Mbedzi MP (2008) The internal variability of the RegCM3 over South Africa. Int J Climatol 28:505–520

Landman W, Seth A, Camargo SJ (2005) The effect of regional climate model domain choice on the simulation of tropical cyclone-like vortices in the southwestern Indian Ocean. J Clim 18:1263–1274

Liang XZ, Kunkel KE, Meehl GA, Jones RG, Wang JXL (2008) Regional climate models downscaling analysis of general circulation models present climate biases propagation into future change projections. Geophys Res Lett 35:L08709, doi:10.1029/2007GL032849

MacKellar NC, Tadross MA, Hewitson BC (2009) Effects of vegetation map change in MM5 simulations of southern Africa's summer climate. Int J Climatol 29:885–898

Mariotti L, Coppola E, Sylla MB, Giorgi F, Piani C (2011) Regional climate model simulation of projected 21st century climate change over an all Africa domain: comparison analysis of nested and driving model results. J Geophys Res 116:D15111, doi:10.1029/2010JD015068

Mason SJ, Jury MR (1997) Climatic variability and change over southern Africa: a reflection on underlying processes. Prog Phys Geogr 21:23–50

McGregor JL (1997) Regional climate modeling. Meteorol Atmos Phys 63:105–117

Mitchell TD, Carter TR, Jones PD, Hulme M, New M (2004) A comprehensive set of high-resolution grids of monthly climate for Europe and the Globe: the observed record (1901–2000) and 16 scenarios (2001–2100). Working Paper 55, Tyndall Centre for Climate Change Research, Norwich

Moufouma-Okia W, Rowell DP (2010) Impact of soil moisture initialization and lateral boundary conditions on regional climate model simulations of the west African monsoon. Clim Dyn 35:213–229

Noguer M, Jones RG, Murphy JM (1998) Sources of systematic errors in the climatology of a nested regional climate model (RCM) over Europe. Clim Dyn 14:691–712

Pal JS, Small EE, Eltahir EAB (2000) Simulation of regional-scale water and energy budgets: representation of subgrid cloud and precipitation processes within RegCM. J Geophys Res 105:29579–29594

Pal JS, Giorgi F, Bi X, Elguindi N and others (2007) The ICTP RegCM3 and RegCNET: regional climate modeling for the developing world. Bull Am Meteorol Soc 88: 1395–1409

Pohl B, Crétat J, Camberlin P (2011) Testing WRF capability in simulating the atmospheric water cycle over equatorial East Africa. Clim Dyn 37:1357–1379

Reason CJ, Jagadheesha D (2005) A model investigation of recent ENSO impacts over southern Africa. Meteorol Atmos Phys 89:181–205

Reason CJC, Landman W, Tennant W (2006) Seasonal to decadal prediction of southern African climate and its links with variability of the Atlantic Ocean. Bull Am Meteorol Soc 87:941–955

Reynolds RW, Rayner NA, Smith TM, Stokes DC, Wang W (2002) An improved *in situ* and satellite SST analysis. J Clim 15:1609–1625

Rossow WB, Schiffer R (1999) Advances in understanding clouds from ISCCP. Bull Am Meteorol Soc 80:2261–2287

Stackhouse PW Jr, Gupta SK, Cox SJ, Mikovitz JC, Zhang T, Chiacchio M (2004) 12-year surface radiation budget data set. GEWEX WCRP News 14:10–12

Staniforth A (1997) Regional modeling: a theoretical discussion. Meteorol Atmos Phys 63:15–29

Stephens GL (2005) Cloud feedbacks in the climate system: a critical review. J Clim 18:237–273

Sylla MB, Gaye AT, Pal JS, Jenkins GS, Bi XQ (2009) High resolution simulations of West Africa climate using regional climate model (RegCM3) with different lateral boundary conditions. Theor Appl Climatol 98:293–314

Sylla MB, Coppola E, Mariotti L, Giorgi F, Ruti PM, Dell' Aquila A, Bi X (2010a) Multiyear simulation of the African climate using a regional climate model (RegCM3) with the high resolution ERA-interim reanalysis. Clim Dyn 35: 231–247

Sylla MB, Dell'Aquila A, Ruti PM, Giorgi F (2010b) Simulation of the intraseasonal and the interannual variability of rainfall over West Africa with a RegCM3 during the monsoon period. Int J Climatol 30:1865–1883

Sylla MB, Gaye AT, Jenkins GS, Pal JS, Giorgi F (2010c) Consistency of projected drought over the Sahel with changes in the monsoon circulation and extremes in a regional climate model projections. J Geophys Res 115: D16108, doi:10.1029/2009JD012983

Sylla MB, Giorgi F, Ruti PM, Calmanti S, Dell'Aquila A (2011) The impact of deep convection on the West African summer monsoon climate: a regional climate model sensitivity study. Q J R Meteorol Soc 137:1417–1430

Tadross MA, Gutowski WJ, Hewitson BC, Jack C, New M (2006) MM5 simulations of interannual change and the diurnal cycle of southern African regional climate. Theor Appl Climatol 86:63–80

Tennant W (2004) Considerations when using pre-1979 NCEP/NCAR reanalyses in the southern hemisphere. Geophys Res Lett 31:L11112, doi:10.1029/2004GL019751

Tomas R, Webster P (1997) The role of inertial instability in determining the location and strength of near-equatorial convection. Q J R Meteorol Soc 123:1445–1482

Tummon F, Solmon F, Liousse C, Tadross M (2010) Simulation of the direct and semidirect aerosol effects on the southern Africa regional climate during the biomass burning season. J Geophys Res 115:D19206, doi:10.1029/2009JD013738

Uppala S, Dee D, Kobayashi S, Berrisford P, Simmons A (2008) Towards a climate data assimilation system: status update of ERA-Interim. ECMWF Newsl 115:12–18

Vigaud N, Richard Y, Rouault M, Fauchereau N (2009) Moisture transport between the South Atlantic Ocean and southern Africa: relationships with summer rainfall and associated dynamics. Clim Dyn 32:113–123

Whitlock CH, Charlock TP, Staylor WF, Pinker RT and others (1995) First global WCRP shortwave surface radiation budget dataset. Bull Am Meteorol Soc 76:905–922

Zeng X, Zhao M, Dickinson RE (1998) Intercomparison of bulk aerodynamic algorithms for the computation of sea surface fluxes using TOGA COARE and TAO data. J Clim 11:2628–2644

Zhang T, Stackhouse PW, Gupta SK, Cox SJ, Mikovitz JC (2009) Validation and analysis of the release 3.0 of the NASA GEWEX surface radiation budget dataset. AIP Conf Proc 1100:597–600

Appendix 1. Additional figures

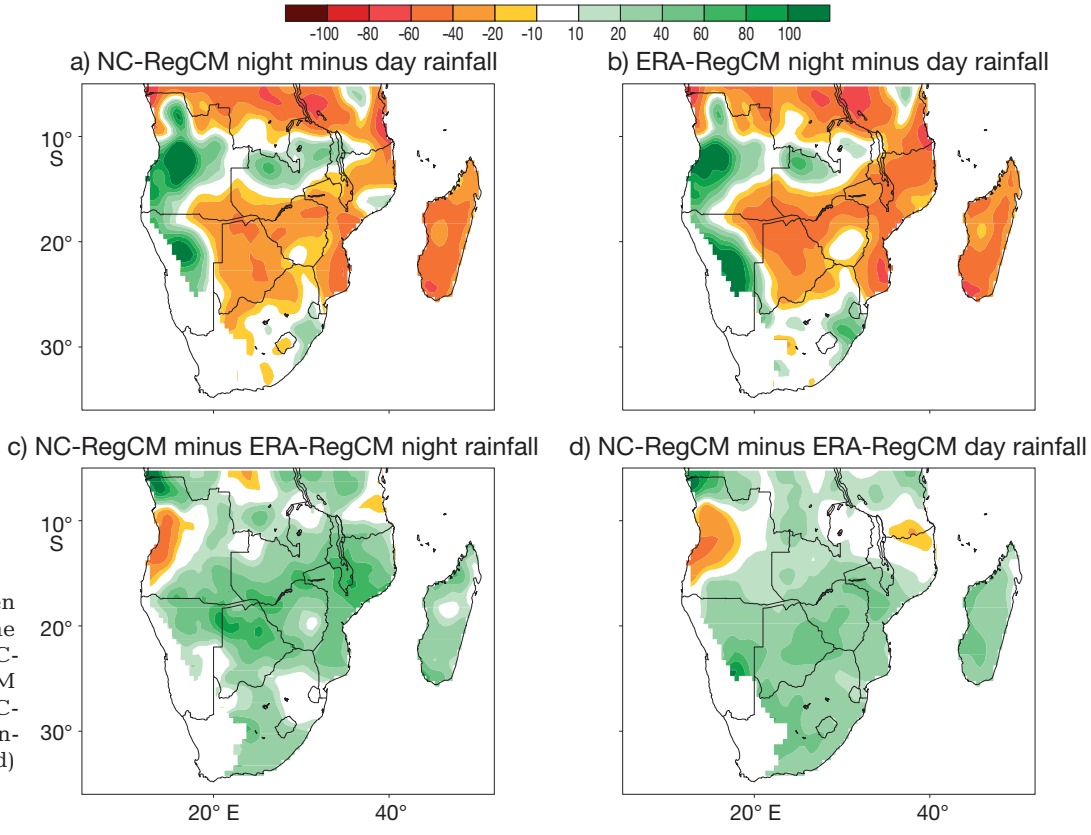

Fig. A1. Difference between the nighttime and daytime rainfall (mm d^{-1}) for (a) NC-RegCM and (b) ERA-RegCM and difference between NC-RegCM and ERA-RegCM rainfall for (c) nighttime and (d) daytime

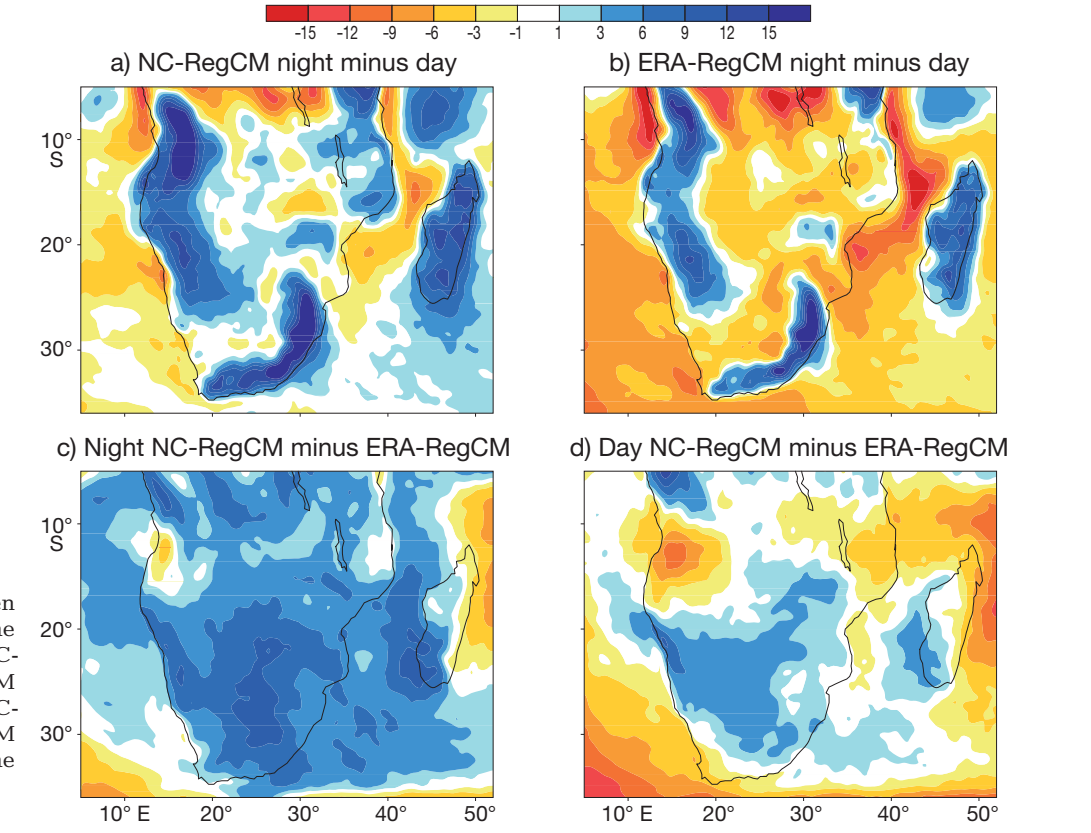

Fig. A2. Difference between the nighttime and daytime cloud cover (%) for (a) NC-RegCM and (b) ERA-RegCM and difference between NC-RegCM and ERA-RegCM cloud cover for (c) nighttime and (d) daytime

Submitted: April 4, 2011; Accepted: August 25, 2011 *Proofs received from author(s): March 12, 2012*